ELSEVIER

Biophysical Chemistry 72 (1998) 37–47

Biophysical Chemistry

Traveling waves in yeast extract and in cultures of *Dictyostelium discoideum*

Stefan C. Müller*, Thomas Mair, Oliver Steinbock

Otto-von-Guericke-Universität, Institut für Experimentelle Physik, Abteilung Biophysik, Universitätsplatz 2, D-39106 Magdeburg, Germany

Revision received 30 January 1998; accepted 13 February 1998

Abstract

Biological self-organization was investigated in a biochemical and a cellular system: yeast extract and cultures of the slime mold *Dictyostelium discoideum*. In both systems traveling reaction-diffusion waves occur in response to oscillatory reactions. Glycolytic degradation of sugar in a yeast extract leads to the spontaneous formation of NADH and proton waves. Manipulation of the adenine nucleotide pool by addition of purified plasma membrane ATPase favors the formation of both reaction-diffusion waves and phase waves. The results indicate that the energy charge has an important impact for the dynamics of glycolytic patterns. When affecting the lower part of glycolysis by pyruvate addition the frequency of wave generation was increased with concomitant formation of rotating NADH and proton spirals. During morphogenesis of the cellular system *Dictyostelium discoideum*, circular and spiral shaped aggregation patterns of motile amoeboid cells form in response to traveling cAMP waves. Velocity analysis of the cell movements reveals that the cAMP waves guide the cells towards the site of wave initiation along optimized trajectories. The minimization of aggregation paths is based on a mechanism exploiting general properties of excitation waves. The resulting aggregation territories are reminiscent of Voronoi diagrams.

Keywords: Oscillatory glycolysis; Morphogenesis; Cell-cell communication; Self-organization

1. Introduction

In biology, oscillatory reactions are often found in processes that play an important role for the control of metabolic and cellular events. Much effort has been made to clarify the impact of such oscillatory reactions on the regulation and coordination of cellular functions. It has been postulated that these can act as cellular clocks and permit frequency encoded information processing [1,2]. During the last decade experimental as well as theoretical studies have shown that oscillatory reactions in biochemical and cellular systems can lead to a new level of spatiotemporal organization, the formation of traveling reaction-diffusion waves. A necessary prerequisite for this kind of self-organization is the coupling of an autocatalytic, e.g. oscillatory, reaction with transport processes such as diffusion. Under these circum-

* Corresponding author. Tel.: +49 391 6718338; fax: +49 391 6711181; e-mail: stefan.mueller@physik.uni-magdeburg.de

0301-4622/98/$19.00
PII S0301-4622(98)00121-5

stances, such diverse events as glycolytic oscillations, calcium oscillations in frog eggs and heart cells and aggregation of amoeboid cells from the slime mold *Dictyostelium discoideum* form traveling waves of a propagator species [3–7], for review see Ref. [8]. Since the wave-generating processes show the characteristics of excitability (threshold value, all or none reaction, refractoriness) the resulting waves are also called excitation waves. Much information about the dynamics and basic principles for the generation of excitation waves has been obtained from investigations of a chemical system, the Belousov–Zhabotinsky (BZ) reaction (cf. Ref. [9]). The velocity v of the excitation waves depends in general on the diffusion coefficient D of the propagator species and the rate constant k of the autocatalytic reaction step according to the relation $v \propto (k D)^{1/2}$. Deviations from the constant velocity of a single planar wave are found in wave trains of high frequency (dispersion) and for curved wave fronts. The velocity deviation Δv caused by a front curvature K is proportional to K as described by the eikonal equation $\Delta v = D K$ for two-dimensional systems. It should thus be noted that significant (and measurable) curvature effects can only occur along highly curved fronts, which typically appear close to pacemakers or during certain wave collisions. Furthermore, excitation waves show, unlike electromagnetic or acoustic waves, no interference and no reflection at boundaries.

The results obtained with the BZ system prove to be a valuable basis for the investigation of biological self-organization, since the dynamics of chemical excitation waves share great similarities with those found in biological systems. As a necessary basis for the search of a biological function of reaction-diffusion waves one has to investigate the mechanisms of biological self-organization. For this purpose we have used two different biological systems where self-organization occurs as a consequence of oscillatory reactions: glycolytic degradation of sugar in a yeast extract as a model for metabolic interactions and cultures of the slime mold *Dictyostelium discoideum* as a model for cell-cell communication.

Regulation of glycolysis in a yeast extract as well as in yeast cells has been the subject of intense experimental and theoretical work, concerning the generation and control of oscillatory glycolytic flux [10–16]. Thus far, a unique picture has not emerged and the control of the oscillatory glycolytic flux is still under debate. Whereas former concepts attribute the main control to a single rate limiting reaction step [17] recent ones favor the concept of metabolic flow control where every reaction step can exert control depending on its control coefficient [18]. The allosteric model proposed by Goldbeter and Lefever [14] focuses on cooperativity and autocatalytic regulation of the phosphofructokinase, where product activation via ADP occurs. This two-variable model reproduces the oscillatory phenomena observed in glycolysis and attributes an important control function to the phosphofructokinase reaction. Extensions of this model to two-dimensional reaction-diffusion processes predict the appearance of traveling waves [19,20], the results of these model calculations being in good agreement with recent experimental results [3]. Introducing a second autocatalytic step into the lower part of glycolysis, similar as in the Sel'kov model [13], produces a variety of dynamic states including chaos [21], which has been also observed experimentally [22,23].

The second system of our investigations is the cellular slime mold *Dictyostelium discoideum* which is one of the classic systems for the study of cell communication and morphogenesis. One of the most successful models for slime mold aggregation was proposed by Martiel and Goldbeter in 1987 [24]. The Martiel–Goldbeter model can be reduced to a two-variable system of ordinary differential equations focusing on the dynamics of extracellular 3′-, 5′-cyclic AMP (cAMP) and a particular state of a high affinity cAMP receptor (cAR1). More recent studies [25] show that the receptor promotes the production of additional cAMP from ATP via the heterotrimeric G protein G2 (and adenylate cyclase. The model was extended by Tyson et al. who included a diffusion term for extracellular cAMP [26]. Despite major simplifications (e.g. the assumption of resting cells) numerical simulations revealed semi-quantitative agreement to experimental data on oscillation periods, wave velocities, and the rotation period of spiral waves [26]. In *Dictyostelium* we find a cAMP-oriented positive chemotaxis coupled to the primary cAMP-wave dynamics [27–30]. This coupling guides the amoebae toward the pacemakers of wave patterns which consequently coincide with the centers of aggregation.

2. Experimental

2.1. Yeast extract

Aerobic growth of the yeast cultures (*Saccharomyces carlsbergensis*, ATCC 9080) and preparation of the yeast extract was performed as described in Ref. [31], except that the phosphate buffer was replaced by 25 mM MOPS, 50 mM KCl (pH 6.5), and that the yeast cells were ground by glass beads in a Braun Melsungen homogenizer. Plasma membrane H^+-ATPase from the yeast *Schizosaccharaomyces pombe* was isolated as described by Dufour et al. for large scale purification [32]. The yeast extract (40 mg of protein/ml, 90 μl) was mixed with 12.5 μl of 1 M trehalose, 6.3 μl of 1 M phosphate (pH 6.5), 4.3 μl of 3 M KCl and 11.3 μl of doubly distilled water (= yeast extract mixture) and then pipetted into a tightly sealed reaction chamber. This reaction chamber was placed into the light beam of a 2D spectrophotometer (λ = 340 nm, cf. Ref. [33]). The spatiotemporal patterns of NADH concentration were monitored by means of a UV-sensitive camera (Hamamatsu C 1000). The resulting movie was stored on a video recorder (SONY time lapse recorder EVT 801 CE). Subsequent image analysis of the digitized movies was done on a SUN SPARC station with the KHOROS program (Version 1.05). For detection of NADH concentration changes the gray levels of a selected image area of 40×40 pixels out of 512×512 pixels were summed up and the arithmetic mean plotted as a function of time. For the detection of proton waves the fluorescent proton indicator fluorescein was added to the yeast extract mixture. The fluorescence was monitored with a Vidicon camera (Hamamatsu C 2400–07) using an inverted microscope (Zeiss IM 35). The excitation light was filtered with a band pass filter at 490 nm and emission was recorded for $\lambda > 520$ nm.

2.2. Dictyostelium discoideum

Cells of *Dictyostelium discoideum*, axenic strain AX-2, were cultivated on nutrient medium and harvested at a density of approximately 5×10^6 cells/ml. The amoebae were then washed three times with buffer and spread uniformly on an agar surface containing 2 mM caffeine. The resulting cell density was measured as approximately 4×10^5 cells/cm^2. The petri dishes were then stored in the dark at 21°C for 4–6 h. It should be noted that recent experimental studies with cAMP mutants indicate that the cAMP signal may not be required for cell aggregation and subsequent fruiting body formation when cell densities are higher than 14×10^5 cells/cm^2 [34].

An inverse microscope (Zeiss IM 35) equipped with a video camera (Hamamatsu C2400) was used for observation of chemotactic cell motion under bright-field illumination. The typical area of observation was 0.39 (0.32 mm^2. Single images and movies were digitized using an image aquisition card (Data Translation DT-2851; 512 (512 pixels; 8 bits gray level).

Velocity analysis was performed with a pixel-based correlation program described earlier [35]. The algorithm does not rely on single cell detection, but analyzes the cross-correlation between the intensity signal $I_{x,y}(t)$ of each pixel site with its neighboring sites $I_{x',y'}(t)$. Assuming that a moving cell causes a characteristic signal, one will find it with a certain retardation time τ in neighboring pixels at a distance Δx. The value of τ is determined from the maximum of the corresponding cross-correlation function, while the value Δx is known from direct calibration. The ratio $\Delta x/\tau$ is an estimate for the local cell velocity. For a detailed description of this methodology see Refs. [27] and [35].

3. Results and discussion

3.1. Traveling waves in a yeast extract

Glycolytic sugar degradation in a yeast extract can be achieved by addition of the disaccharide trehalose and phosphate. The sugar is split via the enzyme trehalase into two units of glucose which enter the glycolytic pathway, whereas phosphate acts as a sink in the lower part of glycolysis. The glucose molecule is degraded to pyruvate and further to ethanol and CO_2 via alcoholic fermentation. It is an energy yielding pathway since 2 moles of ATP are generated per mole of glucose. Glycolysis demonstrates non-linear reaction kinetics by means of autocatalytic reaction steps. Autocatalysis is achieved through feedback activation of the phosphofructokinase by its product

ADP [14]. When there is a coupling of the autocatalytic reaction with diffusion, oscillatory glycolysis is associated with the formation of traveling reaction-diffusion waves. Two-dimensional spectrophotometry of NADH at 340 nm reveals the occurrence of traveling NADH waves 1 h after the onset of glycolysis [3]. The wave velocity amounts to about 5 μm/s, the front width to about 0.7 mm. The waves display mutual annihilation upon collision due to the refractory zone in the back of the wave. This is in accordance with the overall properties of reaction-diffusion waves as exemplified in the chemical BZ reaction. In addition, proton waves with similar shape and propagation dynamics can be observed by means of a fluorescent proton indicator. If these proton waves result from the kinase reactions in the upper part of glycolysis [17], they should precede the NADH waves by about 1.5 mm. This can be estimated from the phase angle between proton and NADH oscillations (87°, Ref. [17]), the period of the NADH-oscillations (20.4 min, see Table 1) and the wave velocity of 5 μm/s. Otherwise, the proton waves represent the NADH-associated proton, so no phase shift would occur.

In another set of experiments the yeast extract was mixed with AMP at the beginning of the measurement. This global increase of the AMP concentration, a positive effector of the phosphofructokinase, leads to the formation of rotating proton spirals evolving from open wave ends (Fig. 1). Remarkably, in the absence of added AMP such open wave ends do not curl up to spiral-shaped waves.

After the first hour of glycolytic degradation of sugar (induction period, see Fig. 2, without pyruvate addition) a transition from bulk oscillations to an excitable yeast extract takes place, where traveling waves are spontaneously generated. The period of the bulk oscillations was measured to be 12 min, subsequent wave formation occurred with a period of 20 min (Table 1, without pyruvate addition). We suggested that accumulation of glycolytic end products and/or intermediates during the first hour is the cause for this process. To test this hypothesis, we tried to accelerate the transition by addition of the glycolytic end product pyruvate from the beginning of the experiment. The results show that pyruvate additions of up to 40 mM did not markedly reduce the duration of the induction period (Fig. 2). A maximum decrease of about 20% in the induction period was observed with 20 mM pyruvate. Thus, accumulation of pyruvate seems not to participate on the emergence of glycolytic excitability. However, two further results show that pyruvate has an important impact for the wave propagation process. First, in its presence open wave ends did form rotating spirals. Second, the period of the wave generation process was reduced whereas the period of the bulk oscillations in the induction period remained unaffected (Table 1). Increasing the pyruvate concentration gradually suppresses the oscillations in the induction period, but wave generation still occurs (Fig. 2). Both pyruvate and AMP induce the formation of rotating NADH and proton spirals from open wave ends. However, whereas pyruvate addition leads to a decrease of the wave generation period, the effect of AMP is just the opposite (Table 1). It should be men-

Table 1
Effect of AMP and pyruvate addition on the period of global oscillations and wave generation

	A	B	C	D	E
Period of global oscillations					
AMP	12.3 ± 1.5	13.0 ± 1.3	13.7 ± 1.7	14.3 ± 1.7	14.1 ± 1.6
Pyruvate	12.3 ± 1.5	11.9 ± 2.1	13.2 ± 2.2	–	
Period of wave generation					
AMP	20.4 ± 2.8	21.7 ± 3.9	22.7 ± 5.8	24.4 ± 4	25.6 ± 5.3
Pyruvate	20.4 ± 2.8	15.7 ± 1.1	12.9 ± 3	14.8 ± 5.1	

The yeast extract mixture (see Section 2) was supplemented with either AMP or pyruvate. NADH concentration changes were monitored by 2D spectrophotometry at 340 nm as described in Section 2. Subsequent gray level analysis of the movies displayed the temporal concentration changes of NADH (compare Fig. 2). The period of the global oscillations and of the spontaneous wave generation was evaluated from these plots. Values represent the mean of two to three independent measurements (±SD) and are expressed per min. The concentrations of the added AMP was A = 0, B = 0.25 mM, C = 0.5 mM, D = 0.75 mM and E = 1 mM. For pyruvate the corresponding values are A = 0, B = 10 mM, C = 20 mM and D = 40 mM. –, not measurable.

tioned that the pyruvate concentrations used to simulate end-product accumulation exceed the concentrations normally measured in a yeast extract (0.6 mM, Ref. [17]).

In general, the formation of rotating spirals from open wave ends depends on the excitability of the system and the length of the refractory zone [36,37]. The higher frequency of wave generation in the presence of pyruvate can be the result of an increased excitability of the yeast extract. The large pyruvate concentration leads to an increased oxidation of NADH via alcohol dehydrogenase and thereby transmits the signal to the glyceraldehyde phosphate dehydrogenase/phosphoglycerate kinase reactions by the NADH oxidation/reduction couple. Moreover, pyruvate also affects the pyruvate kinase reaction [38]. Hence, we suggest that changes in the flow of the lower part of glycolysis can cause an increased excitability of the yeast extract, and that this is the reason why open waves ends form rotating spirals in the presence of pyruvate. On the other hand, AMP addition obviously leads to a decreased excitability (increase of the period, see Table 1), but also induces spiral formation. Due to the activity of the adenylate kinase, AMP addition could result in an enhanced break-down of ATP and thereby to a shortening of the refractory zone in the back of the waves. Another possibility is that the overall increase of adenine nucleotides reduces the effective concentration range where ATP can inhibit the phosphofructokinase. If so, the threshold value for excitation should be increased (decrease of excitability) and the length of the refractory zone in the back of the wave reduced (leading to rotating spirals).

The dephosphorylated adenosine nucleotides AMP and ADP are indicators of a low energetic status of a cell. The fact that AMP leads to a marked change of the propagation dynamics of NADH and proton waves

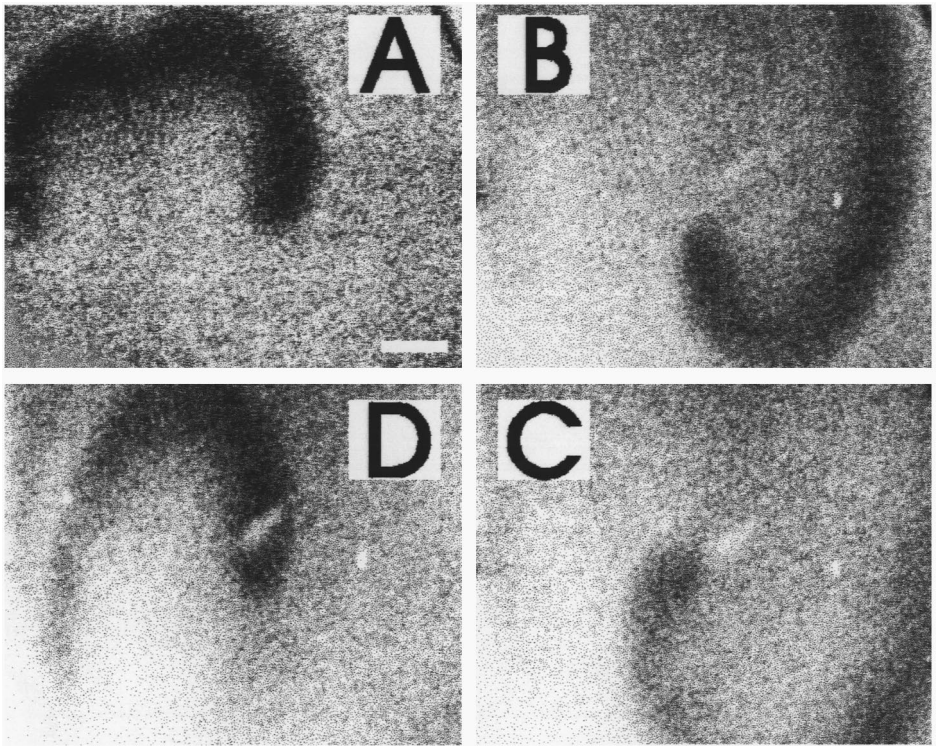

Fig. 1. Rotating proton spiral induced by AMP addition. The yeast extract mixture was prepared as described in Section 2 and supplemented with 0.25 mM AMP. Spatiotemporal changes of the proton concentration were measured by means of the fluorescent proton indicator fluorescein (see Section 2). One hour after the onset of oscillatory glycolysis, spontaneous formation of spiral-shaped proton waves could be observed. (A–D) Single snapshots of a clockwise rotating proton spiral. The time interval between images (A) and (B) is 8 min, between (B) and (C) is 4 min and between (C) and (D) is 8 min. The bar represents 1 mm.

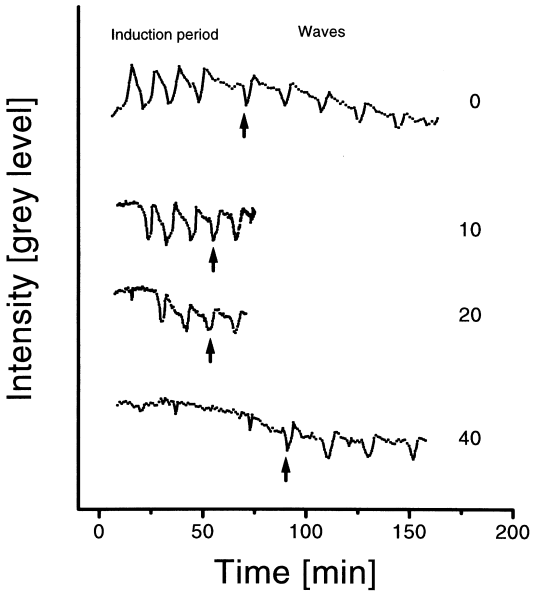

Fig. 2. Effect of pyruvate on the period of glycolytic oscillations. NADH concentration changes in a yeast extract, supplemented with various amounts of pyruvate (0– 40 mM), were measured by 2D spectrophotometry with a UV-sensitive camera as described in Section 2. A small image area of the resulting movie was selected for gray level analysis (see Section 2). The corresponding intensity changes (=NADH concentration) are plotted as a function of time. Visual inspection of the movies revealed that the NADH oscillations were first spatially homogenous (induction period) and thereafter occurred as traveling waves. The time-point where the transition from global oscillations to traveling waves takes place is marked by an arrow.

indicates that the energy charge of the yeast extract is reflected by the pattern dynamics of glycolytic waves. This hypothesis is further supported by the results of experiments where purified plasma membrane ATPase was added to the yeast extract. ATPases split ATP into ADP and phosphate and use the energy liberated by this reaction to perform cellular work. Thus, in the presence of added ATPase, the energy charge of the yeast extract is permanently decreased. Under these experimental conditions, the oscillatory period of the glycolytic flow is only slightly reduced to about 11 min (induction period). The subsequent phase of wave generation is characterized by the appearance of a new wave pattern. Shortly after NADH waves start to propagate through the probe (Fig. 3, at 0s), there occurs a spatially extended overall increase in the concentration of NADH. This overall increase of NADH starts as a diffuse zone in front of the NADH waves (Fig. 3, at 75 s) and subsequently spreads over the whole extract, except past the refractory zone of the NADH wave. The corresponding time-space plot, taken along the line indicated in Fig. 3, at 0s, exemplifies this phenomenon (Fig. 4). A traveling wave starts at the right edge of the probe (middle light line, arrowhead) and propagates through it to about one-third of its length. At the space coordinate marked by an arrow, there is a sudden increase in NADH over the remaining two thirds of the probe's length (middle light line). The velocity of this NADH spreading is about four times faster than that of the wave propagation. We interpret this observation as the occurrence of both, reaction-diffusion waves and phase waves, the former being the result of an excitatory process and the latter of a spatial out-of-phase oscillation of the glycolytic flow.

Due to a concept proposed by Atkinson [39], ATP consuming pathways, i.e. biosynthetic ones, are activated at a high energy charge whereas ATP generating pathways, i.e. catabolism, are activated at a low energy charge. Oscillations then can provide an improved control for the switch between biosynthesis and catabolism (cf. Ref. [40]). The results of this work indicate that this control mechanism might also be extended to spatial phenomena.

Analysis of the phase relationship of the glycolytic intermediates has revealed three different metabolic cross-over points at which control of the oscillatory glycolytic flow can occur, namely at the reaction steps catalyzed by the phosphofructokinase (PFK), glyceraldehyde phosphate dehydrogenase(GAPDH)/phosphoglycerate kinase (PGK) and the pyruvate kinase (PK) [17,41]. In a yeast extract the phase angle with respect to the preceding reaction step is 180° for the PFK, about 60° for the GAPDH/PGK and again 180° for the PK. Interestingly, the phase angle for the GAPDH/PGK is flux dependent [17], serving as a variable that might participate at the transition from oscillations to excitability as shown in Fig. 2. Our results indicate that control of the wave propagation dynamics is exerted by at least two control points. One in the upper part of glycolysis at the PFK step (AMP effect) and one in the lower part of glycolysis at the PK or GAPDH/PGK step (pyruvate effect). Model calculations predict a complex behavior in this case of two control points [21]. In this context the effect of ATPase addition is not only limited to a change of the

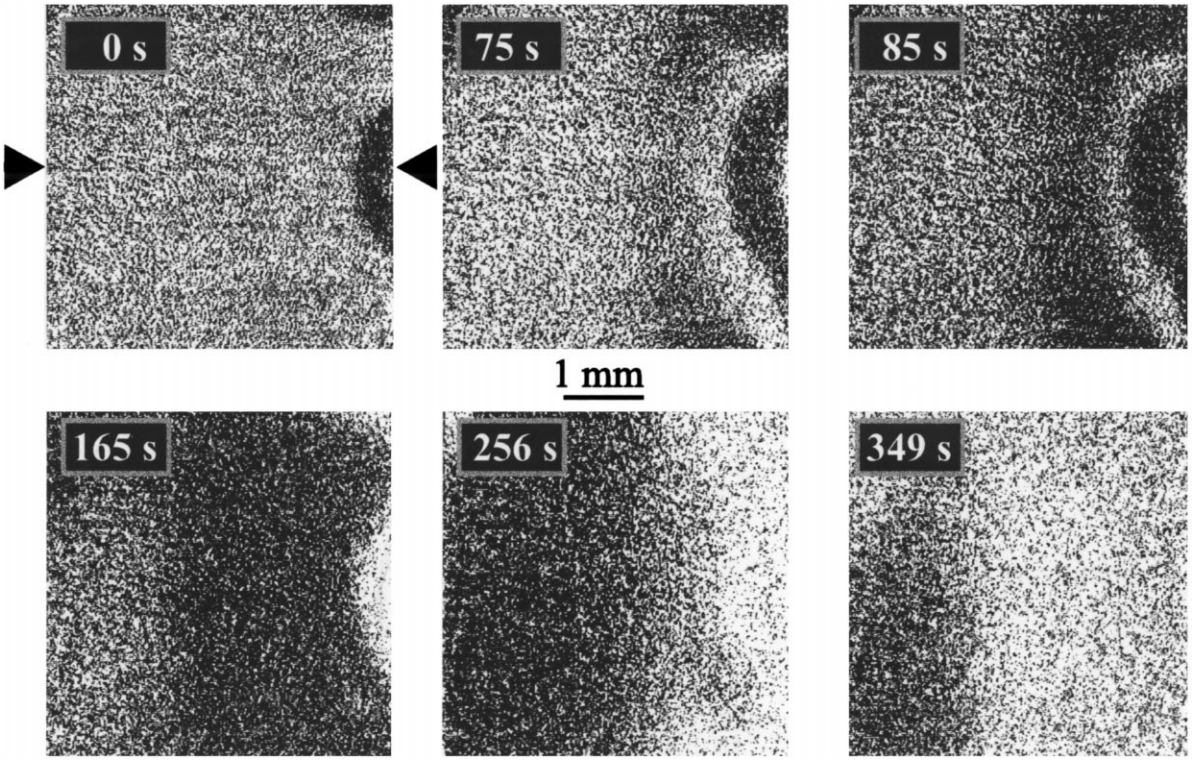

Fig. 3. Phase wave formation in the presence of added ATPase. Purified plasma membrane H^+-ATPase from yeast (0.45 U) was added to the yeast extract mixture. NADH concentration changes were monitored by 2D spectrophotometry at 340 nm (see Section 2). About 1 h after the onset of the experiment, spontaneous formation of traveling reaction-diffusion waves (0-85 s) and phase waves (85–349 s) could be observed. The arrowheads in the image at 0 s indicate the image line along which the time-space plot of Fig. 4 was probed.

energy charge but also to substrate recycling from product at the PK or PGK steps. Such a recycling process can seriously alter the dynamics of a nonlinear system.

A shift of the steady state or the control point might cause the spontaneous formation of traveling waves in the yeast extract as indicated by the observed alteration in the shape of the amplitude (Fig. 2). For the first cycle it is nearly sinusoidal but for the subsequent ones it becomes broadened at the phase of NADH increase, i.e. when the flow through the GAPDH is increased. Waves start to form, when this broadening phase exceeds a critical value. At present we cannot say whether and at which point in the glycolytic reaction sequence a shift of the metabolic control occurs. More experimental data in connection with a theoretical model are necessary to get deeper insight into the process of glycolytic self-organization.

3.2. Waves in Dictyostelium discoideum colonies

The classic methodology for the experimental investigation of excitation waves in the *Dictyostelium* system is dark-field photography [42]. Fig. 5 shows a typical example of a spiral wave pattern obtained by this optical technique during the slime mold aggregation on an agar surface. The figure was generated by superimposing three snapshots recorded with a time-lag of 120 s. The spiral formed under the experimental conditions specified above shows a rotation period and a wavelength of 420 s and 2 mm, respectively. The physical mechanism causing the formation of bright and dark regions is somewhat unclear. Obviously, the amoebae are too large (diameter ~10 μm) to scatter visible light. Also the cell density is known to be homogenous during the earlier stages of aggregation. A possible explanation, however, could

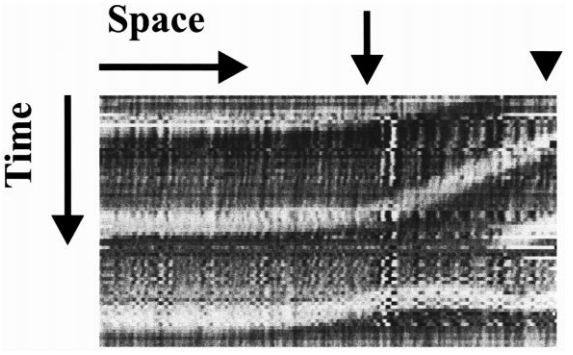

Fig. 4. Time-space plot of the wave patterns shown in Fig. 3. The time-space plot was probed along the image line indicated in Fig. 3 at 0 s. The intensity changes of 72 consecutive images, taken at 30-s intervals, are shown, i.e. the time scale is 36 min. The space scale corresponds to 4 mm. Note that the analysis was performed for three subsequent following waves, i.e. the time period of the time-space plot exceeds that of the images shown in Fig. 3. Increases in NADH concentration appear as light horizontal lines. The middle horizontal line corresponds to the traveling wave shown in Fig. 3. The arrowhead marks the appearance of the traveling NADH wave and the vertical arrow the space coordinate where the fast NADH spreading occurs (see text for further explanation).

be the deformation of the water film covering the amoebae: depending on the shape of cells (round when resting, oblate when moving) the water film could act as a complex lens, thus, refracting the parallel light used for dark-field photography to a varying extent. Fig. 5 also reveals collisions of waves (upper left corner) emitted from different pacemakers. The resulting cusps propagate along curves that mark the boundaries between different aggregation territories. In the following these boundary regions will be analyzed on a microscopic scale.

In a sequence of experiments we have first investigated the cell velocity in microscopic regions with nearly planar cAMP-concentration waves traversing. The results obtained on the basis of cross-correlation analyses showed rhythmic changes in cell velocity varying between approximately 0 and 20–30 μm/min (see also Ref. [27]). The periodicity of velocity oscillations is in agreement with the wave period found from dark-field experiments (typically 6–9 min). The velocity patterns were surprisingly homogenous as could be concluded from histograms of velocity directions. The ratio of wave velocity and cell velocity is usually close to a value of 10:1 with an antiparallel orientation of the corresponding vectors. In agreement with this finding a spinning motion of amoebae was detected close to the center of spiral waves [43]. Similar observations were recently reported by Siegert et al. for 3D mounds which form during the late stages of aggregation [44,45]. The simple fact that chemotactic motion occurs along the direction of normal wave velocities (i.e. perpendicular to the wave front) has interesting consequences. Recently, Steinbock et al. demonstrated an experimental procedure for path finding in labyrinths utilizing chemical waves in the excitable BZ system [46]. Their approach is based on the fact that excitation fronts propagate according to Fermat's principle provided that secondary effects, such as the curvature-velocity dependence, are negligible. By measuring the normal velocities they obtained a vector field from which shortest paths were found from any site in the labyrinth back to the point of wave initiation. It seems obvious that a similar mechanism holds for the chemotactic migration of *Dictyostelium* amoebae. The cells detecting concentration gradients of cAMP are guided along shortest and therefore optimized trajectories towards the pacemaker (i.e. the aggregation center). While this optimization is trivial in homogeneous two-dimensional systems, such as agar surfaces, it might play an important role for survival in heterogeneous 3D systems as given by the natural habitat (soil) of this organism.

Fig. 6a,b now shows a 0.12 mm^2 region with an

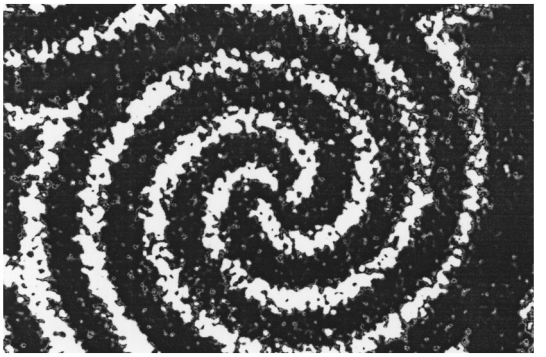

Fig. 5. Superposition of three dark-field photographs of a rotating spiral wave. The snapshots were recorded during the early aggregation phase of the slime mold *Dictyostelium discoideum*. The spiral tip follows a nearly circular trajectory (spiral core). In the upper left corner of the figure the spiral wave collides with waves emitted from a pacemaker located outside the observation area. Time interval between successive snapshots: 120 s.

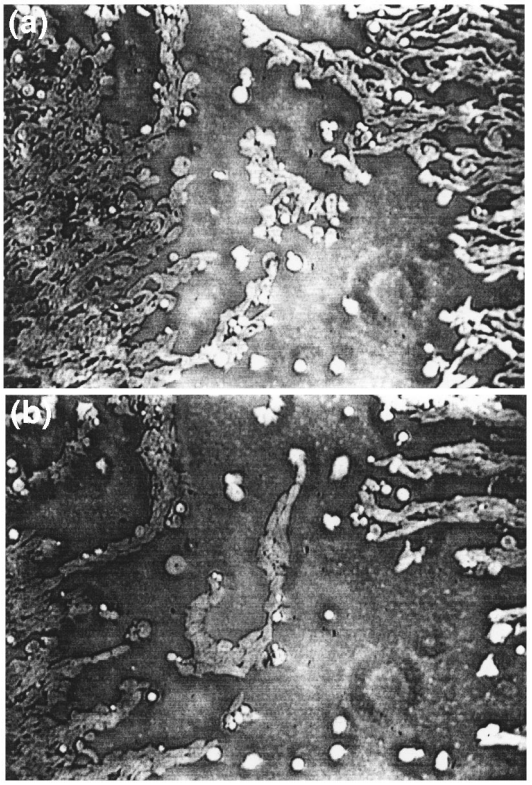

Fig. 6. Two successive microscopic images of aggregating slime mold amoebae. The observation area (0.39×0.32 mm^2) was located along a line of colliding excitation waves. These lines coincide with the boundaries between aggregation territories. The region of low cell density crossing the images in nearly vertical direction increases in width during the course of aggregation. Time interval between snapshots (A) and (B) is 20 min.

aggregation boundary crossing the image along a nearly vertical line. The aggregation boundary appears as a stripe of low cell density. The snapshot given in Fig. 6b was taken 20 min after Fig. 6a. It can be clearly seen that the region of low cell density has increased its width during the time elapsed between the depicted snapshots. A remarkable consequence of the formation of low cell density stripes along aggregation boundaries is that the aggregation territories decouple. The lack of amoebae within the boundary region decreases the excitability until a proper relay of the excitation (i.e. cAMP concentration) becomes impossible. Once the dynamic contact between the adjacent aggregation territories is lost, competition for cells between the corresponding pacemakers, such as the master-slave dynamics of wave sources known from homogeneous reaction-diffusion media, stops. In other words, an information flux between the territories becomes impossible.

Using the correlation-based algorithm described above we extracted the migration velocities for the area presented in Fig. 6. The analysis was based on a sequence of 30 frames recorded with a constant sampling time of 29 s. The resulting vector field of cell velocities is shown in Fig. 7. Each vector represents the velocity obtained by averaging the data in a 51×51 pixel square around its origin. The vector field reveals the existence of two major basins: one on the left side with vectors pointing to the left and one on the right side with vectors pointing to the right. For the separating stripe of low cell density only small or no velocities were detected. The total average of absolute velocities found in the analysis is of the order of 20 μm/min.

The separation of aggregation territories due to collisions of cAMP-concentration waves has also surprising counter-parts in the field of computational geometry. Basic tasks in computational geometry are the nearest neighbor search and the construction

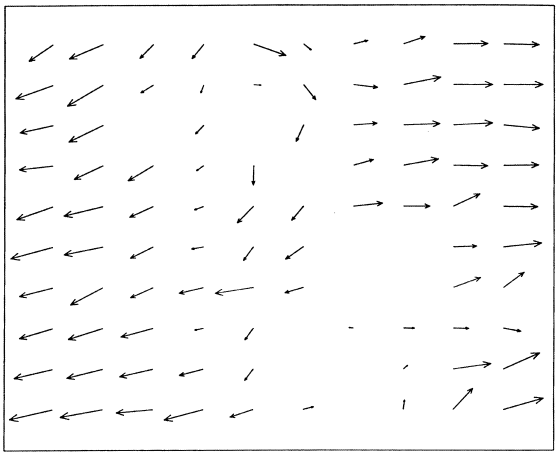

Fig. 7. Vector field of cell velocities as analyzed for the area shown in Fig. 6. The analysis was performed for a 10×10 array of non-overlapping squares (51×51 pixels each). The resulting average velocities are plotted as vectors with their origin centered in the corresponding square. No velocities were determined in certain areas of low or zero cell density. The figure reveals two major migration directions that are in agreement with the qualitative observation of a growing gap between the left and the right cell population (cf. Fig. 6). Image area: 0.39×0.32 mm^2.

of Voronoi diagrams [47]. A Voronoi diagram $Vor(S)$ of a set S of n points p_i in the plane partitions the plane into n equivalence classes, each of which corresponds to a point. Each equivalence class is the Voronoi polygon $V(p_i) = \{r \mid r \in R^2$ and distance$(r, p_i) \leq$ distance$(r, p_j), j \neq i\}$. In other words, the polygon $V(p_i)$ includes all the points that have their shortest distance to p_i rather than to any other point of the set S. Using the divide-and-conquer technique the complete Voronoi diagram of n points in the plane can be constructed in $O(n \log n)$ time, which is also the optimum in the framework of standard methodologies [47]. During slime mold aggregation, both tasks, the nearest neighbor search and the construction of a Voronoi diagram, are solved in a highly parallel fashion. Each cell identifies its nearest aggregation center by means of excitation waves transmitting the relevant information as discussed above. Along the lines of wave collisions (Fig. 6) the cell population consequently constructs the relevant Voronoi polygon and is thus optimizing the entire process of aggregation. Note, that this strategy yields only approximations, since differences in phase and/or amplitude of adjacent pacemakers can introduce deviations from an ideal solution. We would like to emphasize that this optimization would be impossible on the basis of interfering waves. Also a continuous production of a diffusing messenger substance without degradation could not achieve this surprising optimization, since oversaturation of receptors would soon stop the flux of useful information encoded in the local concentration gradient.

4. Conclusions

Traveling waves in yeast extract and in cultures of *Dictyostelium discoideum* share unique features with traveling chemical waves as known from the BZ reaction. This characterizes them as reaction-diffusion waves. Application of the basic principles of chemical excitability is a valuable tool for the analysis and characterization of biological reaction-diffusion waves, as demonstrated by the results of this work and also by others [5,6]. The fact that the propagation dynamics of excitation waves optimize the formation of aggregation centers of *Dictyostelium discoideum* represent an example of how self-organization can be used for biological information processing in cell-cell communication processes. Other examples include the electrical excitation of the heart [48] and the spreading depression in the cortex and the retina [49,50]. Also, the coordination of metabolic processes and transmission of intracellular signals to the environment might be coupled to the dynamics of self-organized structures. NADH and proton waves are candidates for such patterns, although their existence has not been demonstrated yet in living cells. Since several metabolic pathways flow into or branch off the glycolytic pathway, there are multiple possibilities for the coupling of glycolytic excitability to the cell metabolism. Regarding the molecular mechanisms of biological spatiotemporal pattern formation it is interesting to note that the formation of glycolytic waves does not require cellular compartmentation, i.e. transport across biological membranes. The generation of cAMP waves in *Dictyostelium discoideum* cultures is tightly coupled to such transport processes, as is also the case for intracellular calcium waves. Hence, despite the unique validity of the basic principles of chemical excitability for biological self-organization, the particular mechanisms involved can be quite different.

Acknowledgements

We thank Dietrich Kuschmitz from the Max-Planck-Institut Dortmund for providing us purified plasma membrane ATPase and Jörg Schütze for experimental help. T. Mair acknowledges the receipt of a fellowship from the Deutsche Forschungsgemeinschaft.

References

[1] E. Bünning, The Physiological Clock, Springer-Verlag, New York, 1967.
[2] M.J. Berridge, P.H. Cobbold, K.S.R. Cuthbertson, Phil. Trans. R. Soc. Lond. 320 (1988) 325.
[3] T. Mair, S.C. Müller, J. Biol. Chem. 271 (1996) 627.
[4] T. Shinjyo, Y. Nakagawa, T. Ueda, Physica D 84 (1995) 212.
[5] J.D. Lechleiter, D.E. Clapham, Cell 69 (1992) 283.
[6] M.H.P. Wussling, H. Salz, Biophys. J. 70 (1996) 1144.
[7] G. Gerisch, Naturwissenschaften 58 (1971) 430.
[8] B. Hess, Q. Rev. Biophys. 30 (1997) 121.

[9] R. Kapral, K. Showalter (Eds.), Chemical Waves, Patterns, Kluwer, Dordrecht, Netherlands, 1995.
[10] K. Pye, B. Chance, Proc. Natl. Acad. Sci. USA 55 (1966) 888.
[11] A. Boiteux, A. Goldbeter, B. Hess, Proc. Natl. Acad. Sci. USA 72 (1975) 3829.
[12] A. Betz, B. Chance, Arch. Biochem. Biophys. 109 (1965) 585.
[13] E.E. Sel'kov, Eur. J. Biochem. 4 (1968) 79.
[14] A. Goldbeter, R. Lefever, Biophys. J. 12 (1972) 1302.
[15] R. Heinrich, T. A Rapoport, Eur. J. Biochem. 42 (1974) 89.
[16] E. Hofmann, K. Eschrich, W. Schellenberger, Adv. Enzyme Regul. 23 (1985) 331.
[17] B. Hess, A. Boiteux, J. Krüger, Adv. Enzyme Regul. 7 (1969) 149.
[18] B. Teusink, B.M. Bakker, H.V. Westerhoff, Biochim. Biophys. Acta 1275 (3) (1996) 204.
[19] A. Goldbeter, Proc. Natl. Acad. Sci. USA 70 (1973) 3255.
[20] P. Marmillot, J.-F. Hervagault, G.R. Welch, Proc. Natl. Acad. Sci. USA 89 (1992) 12103.
[21] O. Decroly, A. Goldbeter, Proc. Natl. Acad. Sci. USA 79 (1982) 6917.
[22] M. Markus, S.C. Müller, B. Hess, Ber. Bunsenges. Phys. Chem. 89 (1985) 651.
[23] K. Nielsen, P.G. Sørensen, F. Hynne, J. Theor. Biol. 186 (3) (1997) 303.
[24] J.-L. Martiel, A. Goldbeter, Biophys. J. 52 (1987) 807.
[25] P.N. Devreotes, Neuron 12 (1994) 235.
[26] J.J. Tyson, K.A. Alexander, V.S. Manoranjan, J.D. Murray, Physica D 34 (1989) 193.
[27] O. Steinbock, H. Hashimoto, S.C. Müller, Physica D 49 (1991) 233.
[28] F. Siegert, C.J. Weijer, J. Cell Sci. 93 (1989) 315.
[29] P. Foerster, S.C. Müller, B. Hess, Development 109 (1990) 11.
[30] K.J. Tomchik, P.N. Devreotes, Science 212 (1981) 443.
[31] B. Hess, A. Boiteux, Hoppe-Seyler's Z. Physiol. Chem. 349 (1968) 1567.
[32] J.P. Dufour, A. Amory, A. Goffeau, Methods Enzymol. 157 (1988) 513.
[33] S.C. Müller, T. Plesser, B. Hess, Anal. Biochem. 146 (1985) 125.
[34] B. Wang, A. Kuspa, Science 277 (1997) 251.
[35] H. Miike, Y. Kurihara, H. Hashimoto, K. Koga, Trans. IEICE Japan E69 (1986) 877.
[36] A.S. Mikhailov, V.S. Zykov, Physica D 52 (1991) 379.
[37] J.J. Tyson, J.P. Keener, Physica D 32 (1988) 327.
[38] B. Chance, B. Schoener, S. Elsaesser, J. Biol. Chem. 240 (1965) 3170.
[39] D.E. Atkinson, Cellular Energy Metabolism and its Regulation, Academic Press, New York, 1977.
[40] A. Goldbeter, Biochemical Oscillations and Cellular Rhythms, Cambridge University Press, Cambridge, 1996, 83 pp.
[41] K. Kreutzberg, A. Betz, in: I. Lamprecht and A.I. Zotin (Eds.), Thermodynamics and Pattern Formation in Biology, Walter de Gruyter, Berlin, 1988, p. 185.
[42] F. Alcantara, M. Monk, J. Gen. Microbiol. 85 (1974) 321.
[43] O. Steinbock, S.C. Müller, Z. Naturforsch. 50c (1995) 275.
[44] F. Siegert, C.J. Weijer, A. Nomura, H. Miike, J. Cell. Sci. 107 (1994) 97.
[45] J. Rietdorf, F. Siegert, C.J. Weijer, Dev. Biol. 117 (1996) 427.
[46] O. Steinbock, ATóth., K. Showalter, Science 267 (1995) 868.
[47] D.T. Lee, IEEE Trans. Comput. C- 33 (1984) 1072.
[48] J.M. Davidenko, A.M. Pertsov, R. Salomonsz, W. Baxter, J. Jalife, Nature 355 (1991) 349.
[49] E. Sugaya, M. Takato, Y. Noda, J. Neurophysiol. 38 (1975) 822.
[50] M.A. Dahlem, S.C. Müller, Exp. Brain Res. 115 (1997) 319.